Highly-Crystalline Near-Infrared Acceptor Enabling Simultaneous Efficiency and Photostability Boosting in High-Performance Ternary Organic Solar Cells

Hang Yin,[a,‡] Chujun Zhang,[d,‡] Hanlin Hu[b,‡] Safakath Karuthedath,[c] Yajun Gao,[c] Hua Tang,[a] Cenqi Yan,[a] Li Cui,[a] Patrick W. K. Fong,[a] Zhuoqiong Zhang,[d] Yaxin Gao,[e] Junliang Yang,[e] Zuo Xiao,[f] Liming Ding,[f] Frédéric Laquai,[,c] Shu Kong So,[*,d] and Gang Li[*,a]*

a. Department of Electronic and Information Engineering
The Hong Kong Polytechnic University
Hung Hom, Kowloon, Hong Kong SAR, China

b. Shenzhen Key Laboratory of Polymer Science and Technology
College of Materials Science and Engineering
Shenzhen University, 518060, Shenzhen, P.R. China.

c. King Abdullah University of Science and Technology (KAUST)
KAUST Solar Center (KSC)
Physical Sciences and Engineering Division (PSE)
Material Science and Engineering Program (MSE)

Thuwal 23955-6900, Kingdom of Saudi Arabia

d. Department of Physics and Institute of Advanced Materials

Hong Kong Baptist University

Kowloon Tong, Hong Kong SAR, P.R. China

e. Key Laboratory for Super-microstructure and Ultrafast Process

School of Physics and Electronics

Central South University, Changsha, P. R. China.

f. Center of Excellence in Nanoscience (CAS)

Key Laboratory of Nanosystem and Hierarchical Fabrication (CAS)

National Center for Nanoscience and Technology

Beijing, 100190, P. R. China

KEYWORDS: organic solar cell; photostability; ternary solar cell; near-infrared acceptor

ABSTRACT: The near-infrared (NIR) absorbing fused-ring electron acceptor, COi8DFIC, has demonstrated very good photovoltaic performance when combined with PTB7-Th as donor in binary organic solar cells (OSCs). In this work, the NIR acceptor was added to state-of-the art PBDB-T-2F:IT-4F-based solar cells as a third component, leading to: (i) an efficiency increase of the ternary devices compared to the binary solar cells in the presence of the highly-crystalline COi8DFIC acceptor and (ii) much improved photostability under 1-sun illumination. The electron transport properties were investigated and revealed the origin of the enhanced device performance.

Compared to the binary cells, the optimized ternary PBDB-T-2F:COi8DFIC:IT-4F blends exhibit improved electron transport properties in the presence of 10% COi8DFIC, which is attributed to improved COi8DFIC molecular packing. Furthermore, transient absorption spectroscopy revealed slow recombination of charge carriers in the ternary blend. The improved electron transport properties were preserved in the ternary OSC upon aging, while in the binary devices they seriously deteriorated after simulated 1-sun illumination of 240 hours. Our work demonstrates a simple approach to enhance both OSC efficiency and photostability.

Introduction

The development of solution-processed organic solar cells (OSCs) has attracted considerable attention, as OSCs are considered a next generation photovoltaic technology, which offers manufacturing of lightweight, low-cost, and flexible solar cell panels.[1-7] In the early days of bulk heterojunction (BHJ) OSCs, the donor material mainly contributed to the light absorption and hole transport, whereas the fullerene acceptor material usually transported electrons.[8-12] After remaining on a low efficiency level for more than two decades, the power conversion efficiency (PCE) of donor:acceptor (D:A) BHJ solar cells has now exceeded 15%, following the milestone BHJ OSC devices based on generations of donors such as MDMO PPV, P3HT, PTB7, DPP family, PBDB-T family etc.[13-16] The full names of materials in this work are summarized in the Supporting Information. In general, to achieve high PCE in OPV devices, low-bandgap and high carrier mobility materials with suitable energy level alignment are used and processing conditions such as solvent additives and postproduction annealing are employed to optimize the morphology

of the donor-acceptor BHJ.[17-20]

Besides efficiency, stability is a main challenge for the commercialization of OSC devices.[21-25] Among BHJ solar cells, PBDB-T-2F-based (PM6-based) devices are at the forefront of state-of-the-art PCEs, whereas the device stability is much less studied. However, it is necessary to fabricate high-performance and photo-stable solar cells. In this paper, we report a fused-ring electron acceptor (FREA) - COi8DFIC incorporated as a third component in ternary solar cells to improve both the device efficiency and photostability of PBDB-T-2F:IT-4F BHJ solar cells. In ternary OSCs or hybrid devices, near-infrared acceptors (NIAs) have often been used to absorb longer wavelength photons and thereby to increase the short-circuit current density (J_{sc}).[26,27] COi8DFIC is an excellent NIA which not only has a very low bandgap (photoresponse up to 1000 nm), but also has demonstrated one of the highest PCEs in OSCs to date. It is composed of a fused thienothiophene central moiety and di-fluoro-substitued indene-diylidene-dimalononitrile terminal groups.[28] The synthesis follows the methods in Ref. 28: CO8-CHO (100 mg) was first mixed with 2-(5,6-difluoro-3-oxo-2,3-dihydro-1H-inden-1-ylidene)malononitrile (100 mg) in $CHCl_3$, and pyridine (0.7 ml) was added and the mixture was stirred for 12h at room temperature and purified by column chromatography as $CHCl_3$ eluent to form COi8DIFC as black solid (75 mg, 60%) Here, we observe that the highly-crystalline NIA COi8DFIC not only extends the light harvesting properties of PM6:IT-4F blends when added as a third component, leading to improved J_{sc} and PCE. Surprisingly, it also acts as a stabilizer for solar cells exposed to solar illumination conditions. The chemical structures of IT-4F and the NIA COi8DFIC are depicted in **Figure 1(a)**. The optimized ternary PBDB-T-2F:IT-4F:COi8DFIC solar cells show an enhanced PCE of 13.7% compared to 12.3% of the

binary PBDB-T-2F:IT-4F device, and still maintain a high efficiency of 11.6% after exposure to 1-Sun illumination for 240 hours (15% drop), when 10% COi8DFIC were present as acceptor. In contrast, the efficiency of the binary PBDB-T-2F:IT-4F device drops rapidly to below 5% during the same period (corresponding to a 60% PCE reduction). Charge carrier transport measurements indicate that the ternary BHJs with COi8DFIC exhibit improved electron transport properties, a consequence of improved COi8DFIC molecular packing in ternary blends film, as evidenced by GIWAXS. Furthermore, transient absorption (TA) spectroscopy on thin film binary and ternary blends indicates less geminate recombination and slower non-geminate charge carrier recombination in the ternary OSC.

Results and Discussion

First, we fabricated binary OPV devices with a fixed D:A weight ratio of 1:1, and the device structure is ITO/PEDOT:PSS/BHJ/PFN-Br/Ag. Figure 1(b) shows the current density - voltage (JV) characteristics of the optimized binary PBDB-T-2F:IT-4F and PBDB-T-2F:COi8DFIC BHJ solar cells under 100 $mWcm^{-2}$ AM1.5G illumination. For the PBDB-T-2F:IT-4F cell, an overall PCE of 12.3% is achieved, with J_{sc} of 20.3 mA/cm^2, fill factor (FF) of 70.3%, and V_{oc} of 0.837 V. The corresponding binary PBDB-T-2F:COi8DFIC device achieved a PCE of 7.5%, with J_{sc} of 14.8 mA/cm^2, FF of 63.3%, and V_{oc} of 0.797 V.

Next, ternary OPV BHJ devices with two acceptors were fabricated. As shown in Figure 1(c), the absorption spectra of binary PBDB-T-2F:IT-4F and PBDB-T-2F:COi8DFIC BHJ films exhibit different peaks. Therefore, we expected that addition of COi8DFIC to the PBDB-T-2F:IT-4F blend

would lead to additional absorption, specifically in the near-infrared spectral region. The JV curves of PBDB-T-2F-based solar cells with various IT-4F/COi8DFIC weight fractions are shown in Figure 1(b). The PCE-optimized weight ratio is 1:0.9:0.1 for the PBDB-T-2F:IT-4F:COi8DFIC ternary blend. The ternary device exhibits a significantly improved PCE of 13.7%, with J_{sc} of 22.1 mA/cm^2, FF of 75.2%, and V_{oc} of 0.825 V. **Table 1** summarizes all performance parameters of binary and ternary OPV devices with different acceptor compositions. Figure 1(d) shows the external quantum efficiency (EQE) spectra of optimized PBDB-T-2F:IT-4F:COi8DFIC ternary solar cells and their binary counterparts. In line with the absorption spectra of the ternary films, the EQE spectra show improved photoresponse in the near-infrared region, leading to an increased current density of the ternary devices.

Space-charge-limited current (SCLC) measurements were performed to evaluate the electron mobilities in binary and optimized ternary BHJs. The structure of the electron-only device is ITO/Al/BHJ/LiF/Al, and the Al layer blocks the hole carriers.[29-31] **Figure 2** (a, b) shows the JV characteristics of the binary PBDB-T-2F:IT-4F, PBDB-T-2F:COi8DFIC and the optimized ternary BHJs at different temperatures. The hole mobilities can be extracted by the space-charge-limited current (SCLC) model. The zero-field single-carrier mobilities μ_0 of thin films (BHJ or pure materials) can be fitted by the SCLC model

$$J = \frac{9}{8} \cdot \varepsilon_0 \varepsilon_r \mu_0 \exp(0.89\beta\sqrt{F})(\frac{V^2}{L^3}) \quad (1)$$

where $\boldsymbol{\varepsilon_r}$ is the medium permittivity, $\boldsymbol{\mu_0}$ is the zero-field carrier mobility $\boldsymbol{\varepsilon_0}$ is the dielectric constant in vacuum, $\boldsymbol{L}$ is the thickness of the film under test, J is the current density, F is the applied electric field, V is the applied voltage, and $\boldsymbol{\beta}$ is the Poole-Frenkel (PF) slope. The JV-derived energetic disorder $\boldsymbol{\sigma_e}$, and high-temperature limited carrier mobilities $\boldsymbol{\mu_\infty}$ can be obtained by

measuring $\boldsymbol{JV}$ curves at different temperatures. In the low electric field region, blending of COi8DFIC increases the current response, and the zero-field electron mobilities $\boldsymbol{\mu_{0,e}}$ of the binary and ternary BHJs reach 6.4×10^{-6} and 2.6×10^{-5} $cm^2V^{-1}s^{-1}$, respectively. $\boldsymbol{\mu_{0,e}}$ of the PBDB-T-2F:COi8DFIC BHJ is 3.6×10^{-6} $cm^2V^{-1}s^{-1}$. (**Figure S1**) Meanwhile, as shown in **Figure S2**, zero-field hole mobilities $\boldsymbol{\mu_{0,h}}$ of the PBDB-T-2F:IT-4F and the optimized ternary BHJs are 8.3×10^{-5} and 3.9×10^{-5} $cm^2V^{-1}s^{-1}$, respectively, with the hole-only structure of ITO/PEDOT:PSS/BHJ/Spiro-TPD:CuPc/Au. The Gaussian disorder model (GDM) was used to evaluate the energetic disorder of the electron transport $\boldsymbol{\sigma_e}$, which is expressed as[32,33]

$$\boldsymbol{\mu_0 = \mu_\infty exp\left[-\left(\frac{2\sigma_e}{3kT}\right)^2\right] \exp\left(\beta\sqrt{F}\right)} \quad (2)$$

where $\boldsymbol{k}$ is the Boltzmann constant, T is the device temperature, and $\boldsymbol{\mu_\infty}$ can be extracted from the y-intercept from the plot of $\boldsymbol{\mu_0}$ against $1/T^2$.[(Figure 2(c)] The optimized ternary BHJ exhibits improved $\boldsymbol{\mu_{0,e}}$ at different temperatures. $\boldsymbol{\sigma_e}$ values decrease from 91 meV in the binary BHJ to 73 meV in the optimized ternary BHJ. The optimized ternary BHJ with 10 wt% COi8DFIC exhibits negligible Poole-Frenkel (PF) effect. In organic semiconductors, a large proportion of electrons are trapped in localized states, and only few can be de-trapped and contribute to the overall conductivity facilitated by the thermal energy. However, an external electric field F can provide the required activation energy. Usually, values of the PF slopes are positive as F supports the energy for trapped electrons to be de-trapped rather than the thermal energy. However, large $\boldsymbol{\beta}$ values are unfavourable for the charge carrier transport in BHJs, especially in the low-field region, due to large energetic barriers for charge hopping. As shown in Figure 2(d), the PF slope $\boldsymbol{\beta}$ of the ternary BHJ are in the range of ~0-4.0×10^{-4} $(cm/V)^{1/2}$ at different temperatures, whereas $\boldsymbol{\beta}$ values

are much higher in the binary control sample, 1.7-4.2×10^{-4} $(cm/V)^{1/2}$). The Poole-Frenkel slope $\boldsymbol{\beta}$ can be extracted from the mobility curves by $\boldsymbol{\mu(F) = \mu_0 \exp\left(\beta F^{1/2}\right)}$. A small (or negative) $\boldsymbol{\beta}$ indicates that shallow energetic barriers exist in the forward direction, which is favorable for electron transport. Therefore, the introduction of the ternary component COi8DFIC successfully improves the electron transport in PBDB-T-2F:IT-4F BHJs, and thereby the corresponding OPV devices exhibit enhanced FFs and PCEs.

Figure S3 shows the height and phase images of the binary PBDB-T-2F:IT4F and PBDB-T-2F:COi8DFIC and optimized ternary PBDB-T-2F:IT-4F:COi8DFIC films from atomic force microscopy (AFM). The root mean square roughness (Rq) values of the two binary BHJs are 2.2nm and 2.1nm, respectively, and the introduction of 10% COi8DFIC into the PBDB-T-2F:IT4F binary blends further decreases Rq in PBDB-T-2F:IT4F:COi8DFIC (1:0.9:0.1) to 1.9nm. The AFM phase images show that the ternary blend is not only uniform, but also contains a nanofibrillar network, which is advantageous for charge transport and charge collection.

In order to obtain more insights regarding the molecular packing in the blend films, grazing-incidence wide angle X-ray scattering (GIWAXS) has been applied to characterize the orientation and crystallinity for binary blend films: PBDB-T-2F:IT-4F and PBDB-T-2F:COi8DFIC as well as the ternary PBDB-T-2F:IT-4F:COi8DFIC blend films. As shown in **Figure 3**, for the PBDB-T-2F:IT-4F binary blend film, an obvious (010) scattering peak is noticed from the 2D GIWAXS pattern in the Z direction, which is due to the strong π-π out-of-plane stacking in the blend film. To distinguish the scattering feature of the two components in the blend film, both pure PBDB-T-2F and pure IT-4F films were also examined by GIWAXS (Supporting Information). Since IT-4F exhibits negligible diffraction in the long *q* regime as shown in the Supporting Information, the

strong (010) scattering peak at ca. 1.76 $Å^{-1}$ in the PBDB-T-2F:IT-4F blend film is ascribed to PBDB-T-2F instead, which also agrees with the scattering features of a pure PBDB-T-2F film. A Lamellar diffraction ring (100) is also observed for a PBDB-T-2F: IT-4F binary BHJ film at ca. 0.31 $Å^{-1}$. Different from the PBDB-T-2F: IT-4F film, the PBDB-T-2F:COi8DFIC binary film shows two lamellar scattering peaks from the 2D GIWAXS pattern: the one located at smaller q corresponding to PBDB-T-2F and the one at larger q is from COi8DFIC. Also, distinct scattering peaks emerge, which are ascribed to the pure COi8DFIC component, evidenced by the pure COi8DFIC film scattering features as shown in the Supporting Information (**Figure S4**). Interestingly, the second (0.88 $Å^{-1}$) and third scattering peak (1.32 $Å^{-1}$) in the Z direction showed up for the lamellar (100) scattering peak at larger q, namely 0.44 $Å^{-1}$, which was not seen in the PBDB-T-2F:COi8DFIC binary system. This indicates a better packing of COi8DFIC molecules in the ternary blend film. This improved COi8DFIC molecular packing can explain the increased charge carrier transport in the ternary blend film as discussed above.

To reveal the photophysical processes following photoexcitation, we performed nanosecond-microsecond transient absorption (ns-µs TA) spectroscopy on both binary and ternary blend films. **Figure 4** shows the ns-µs TA spectra of binary and ternary blend films measured at a fluence of ~13 µJ/cm^2. Herein, negative signals represent photo-induced absorption (PA) and positive signals transient photo bleaching (PB) of the sample. Figure 4a shows the ns-µs spectra of a ternary blend film. We assigned the PA1 (~1280-1350 nm), PA2 (~1130-1210 nm), and PA3 (~920-980 nm) bands of the TA spectra to the charge-induced absorption of carriers in COi8DFIC, PBDBT-2F, and IT4F, respectively. This assignment is based on a comparison of the spectral features monitored in binary and ternary blend films. Clearly, PA1 band is absent in the ns-µs TA spectra of PBDBT-2F:IT4F blends (Figure 4b), hence PA1 was assigned to charge carriers residing on

COi8DFIC in the ternary blend film (Figure 4a). Figure 4c shows the TA spectra of PBDBT-2F:COi8DFIC binary blends. Here, the PA3 band, which is observed in the ns-µs TA spectra of the ternary blend, is absent. Thus, we assigned the PA3 band to the charge-induced absorption of carriers residing in the acceptor IT4F. All blends exhibit the PA2 band, consequently it is ascribed to charge-induced absorption of carriers in the donor polymer, PBDBT-2F. The assignment of the PB signals was done by comparing the spectra of the ternary blend with the TA spectra measured on neat films of each material (see **Figure S5**). Precisely, the PB1 (~840-900 nm), PB2 (~610-680 nm), and PB3 (~780-810 nm) bands are assigned to the photobleaching of COi8DFIC, PBDBT-2F, and IT4F, respectively. To further analyze the carrier recombination, we measured the fluence dependence of the charge carrier decay dynamics of all three blend systems (Figures 4d-f). Fluence dependent charge carrier decays are observed for both PBDBT-2F:IT4F blends and the ternary blend, indicating that charges are separated and undergo non-geminate recombination. On the other hand, largely fluence independent decay dynamics are observed for PBDBT-2F:COi8DFIC blends, pointing to trap-assisted recombination.[34] We parametrized the decay dynamics using a previously reported two-pool recombination model to quantify the fraction of charge carriers undergoing geminate and non-geminate recombination.[35] The fits demonstrate close-to-unity charge separation efficiency in the ternary system, while the binary blends PBDBT-2F:IT4F and PBDBT-2F:COi8DFIC exhibit 90% and 60% charge separation efficiency, respectively, as indicated in Figure 5. Further details of the fit can be found elsewhere.[36] We note that this is in line with the different J_{sc} of devices. We hypothesize based on the GIWAXS results (vide supra) that enhanced packing of molecules in the ternary blend facilitates charge separation and transport, so that charge carriers can be extracted at the electrodes before they recombine.

The photostability of the ternary PBDB-T-2F:IT-4F:COi8DFIC devices was evaluated and compared with the PBDB-T-2F:IT-4F binary device. Solar cells were encapsulated in a glove box, transferred to ambient air, and then exposed to illumination from white-light LED array with an irradiance equivalent to 1-Sun (100 mW/cm^2). **Figure 5** shows the measured OPV performance parameters of the binary and ternary BHJ solar cells containing 10 wt.% COi8DFIC as a function of the exposure time. Apart from the improved PCE, the ternary device also exhibits remarkably enhanced photostability compared to the binary device. After a 240-hour illumination, the ternary PBDB-T-2F:IT-4F:COi8DFIC device still exhibits a PCE of 11.6%, with J_{sc} of 20.9 mA/cm^2, V_{oc} of 0.82 V, and FF of 67.1%, equivalent to ~85% of its initial PCE. In contrast, the efficiency of the binary PBDB-T-2F:IT-4F device decreased to 4.7% during the same period. Although COi8DFIC is only 10% of total acceptors in the ternary blend, we also fabricated the binary PBDB-T-2F:COi8DFIC OPV device, which shows an optimized but lower fresh PCE of 7.5% (Table 1). As shown in **Figure S6**, the photostability is better than that of the PBDB-T-2F:IT-4F binary cell: after a 240-hour illumination, the PCE had decayed to 5.5% (~73% of the initial PCE), however, both binary solar cells had inferior photostability than the optimized ternary device. This clearly indicates that the significantly enhanced photostability of the ternary device is not simply due to the stable third component COi8DFIC.

We therefore further evaluated the BHJ film properties after exposure to 1-Sun illumination. **Figure 6**(a,c) shows the EQE spectra and JV curves of the binary PBDB-T-2F:IT-4F and ternary (10 wt% COi8DFIC) BHJ solar cells before and after illumination of 120 hours.. After illumination, the EQE response of the binary PBDB-T-2F:IT-4F BHJ significantly declined, resulting in a reduced J_{sc}. Figure 6 (b) plots the EQE values ratio before and after a 120-hour 1-Sun illumination of the binary and optimized OSCs as a function of wavelength. Clearly, the ternary BHJ retains

high EQE values in the range of ~400-750 nm, where mainly the donor polymer absorbs, compared to the binary device. Furthermore, as shown in Figure 6(d), the ternary BHJ retains $\boldsymbol{\mu_{0,e}}$ of 2.4×10^{-5} $cm^2V^{-1}s^{-1}$, whereas the electron mobility of the binary BHJ was reduced to $\boldsymbol{\mu_{0,e}} = 2.8\times10^{-6}$ $cm^2V^{-1}s^{-1}$ after the electron-only devices had been exposed to 1-Sun illumination for 120 hours. Thus, the highly-crystalline NIA COi8DFIC not only contributes to light harvesting in ternary (and potentially also tandem) organic solar cells, but also stabilizes the BHJ leading to retention of high EQE values and virtually unchanged electron transport properties when solar cells are exposed to more than hundred hours of solar illumination.

Conclusions

In this work, we demonstrate that the near-infrared absorbing, electron-accepting small molecule acceptor COi8DFIC simultaneously improves the OPV performance and photostability in PBDB-T-2F:IT-4F:COi8DFIC ternary devices. Precisely, COi8DFIC improves the PCE in two ways: firstly, by extending the BHJ's absorption to the NIR spectral region and secondly, by enhancing the electron transport properties of the BHJ. Consequently, the optimized ternary BHJ containing 10 wt.% COi8DFIC exhibits an impressive PCE of 13.7% and it largely maintains its high efficiency after exposure to 1-sun illumination for 240 hours. In contrast, the efficiency of binary PBDB-T-2F:IT-4F devices drops to below 5% during the same period. The reasons for the performance and stability increase were investigated by GIWAXS and transient absorption spectroscopy. Increased packing of molecules and more efficient charge separation were observed in the ternary blend, explaining the trend in short circuit currents and device performance. In conclusion, we demonstrate that the NIR acceptor COi8DFIC is an excellent candidate for fabrication of high-performance photo-stable ternary OPV devices.

Experimental Section

OPV Device Fabrication: The device structure was ITO/PEDOT:PSS/BHJ/PFN-Br/Al. A glass substrate with a pre-patterned ITO (sheet resistance ~ 15 Ω sq^{-1}) was ultrasonicated subsequently in deionized water (DI-water), acetone, and isopropanol. The cleaned substrates were cleaned by UV-ozone treatment for 15 min. PEDOT:PSS solution was spin-coated on the substrates at 6000 rpm for 30 s, and were then placed on a hot plate at 150 °C for 10 mins. After cooled to room temperature, the substrates were sent to an N_2 filled glove box. The PBDB-T-2F and acceptor materials IT-4F and COi8DFIC were blended at an overall D:A weight ration of 1:1, and the materials were dissolved in chlorobenzene (CB) with a donor concentration of 10 mg/mL (1 vol% 1,8-diiodooctane). A blend film PBDB-T-2F:IT-4F:COi8DFIC with various D:A1:A2 weight ratio was prepared by spin-coating at 3000 rpm for 60 s, and then post-annealed at 150 ºC for 10 mins. PFN-Br solution (1.0 mg/mL in methanol) was spin-coated on the top of BHJ layers at 3000 rpm for 30 s. Finally, a 90 nm silver cathode deposited by using thermal evaporation.

SCLC Measurement: Single-carrier (electron-only) devices were measured under low vacuum conditions (<30mbar) in a Cryostat (Model Oxford Instruments DN-V). Before carrier mobility measurements, the Cryostat chamber was evacuated by a vacuum pump (Model Edwards RV3) for at least 12 hours. A temperature controller (Model Oxford Instruments ITC 502) was connected into the Cryostat chamber to monitor and regulate the temperature. The real temperature of the sample under test was calibrated independently by a thermal couple which is connected to the sample directly. For the cooling process, liquid nitrogen (N_2) (boiling point of 77K) was filled into the N_2 bath, and the chamber temperature was regulated by a temperature controller. The waiting time was 40 minutes to stabilize sample temperature. Charge carriers can be injected into the thin-film active layer by the applied DC voltage through a source measure unit (SMU) Keithley (Model

236). The SMU was also used to record the currents under different voltage conditions. The curve of the applied voltages and the corresponding currents was plotted by the software Origin 8.0.

GIWAXS: Measurements were carried out with a Xeuss 2.0 SAXS/WAXS laboratory beamline using a MetalJet-D2, Excillum (0.134144 nm) and a Pilatus3R 1M detector. The incidence angle is 0.2°, beam size is 0.8 by 0.8 mm2, exposure time is 3600 s.

AFM: Atomic Force Microscopy studies were carried out using Bruker's Dimension Icon Atomic Force Microscope (AFM) in Si tapping mode. AFM quantitative morphological analysis was performed using AutoMet AFM software.

TA Spectroscopy: TA spectroscopy was carried out using a home-built pump-probe setup. A fraction of the output of a commercial titanium:sapphire amplifier (Coherent LEGEND DUO, 4.5 mJ, 3 kHz, 800 nm, 100 fs) was focused into a c-cut 3 mm thick sapphire window, thereby generating a white-light supercontinuum from ~550 to ~1700 nm. The excitation light (pump pulse) was provided by an actively Q-switched Nd:YVO_4 laser (INNOLAS picolo AOT) frequency-doubled to provide <1 ns (FWHM) pulses at 532 nm. A detailed TA experimental description can be found elsewhere.[34]

Table 1. Figures-of-merit of OPV devices using PBDB-T-2F:IT-4F, PBDB-T-2F:COi8DFIC, and ternary blends with different acceptor weight compositions as photoactive layer at 100 mW·cm^{-2} AM1.5G illumination. Values in parentheses are averages of 4-8 devices.

COi8DFIC Content (wt%)	V_{oc} (V)	J_{sc} (mA/cm^2)	FF (%)	PCE (%)
0	0.839±0.002 (0.837)	20.6±0.2 (20.9)	69.4±1.1 (70.3)	12.0±0.2 (12.3)
10	0.830±0.004 (0.825)	21.7±0.4 (22.1)	73.9±0.8 (75.2)	13.3±0.3 (13.7)
30	0.832±003 (0.834)	20.4±0.3 (20.5)	76.0±0.9 (76.6)	12.9±0.2 (13.1)
50	0.818±0.002 (0.819)	20.5±0.1 (20.3)	68.1±1.3 (69.7)	11.4±0.2 (11.6)
70	0.816±0.003 (0.821)	18.7±0.3 (19.0)	64.0±0.4 (64.4)	9.8±0.1 (10.0)
90	0.793±0.002 (0.789)	15.0±0.3 (15.4)	63.1±0.5 (63.0)	7.5±0.1 (7.6)
100	0.790±0.005 (0.797)	14.5±0.4 (14.8)	61.6±1.0 (63.3)	7.1±0.3 (7.5)

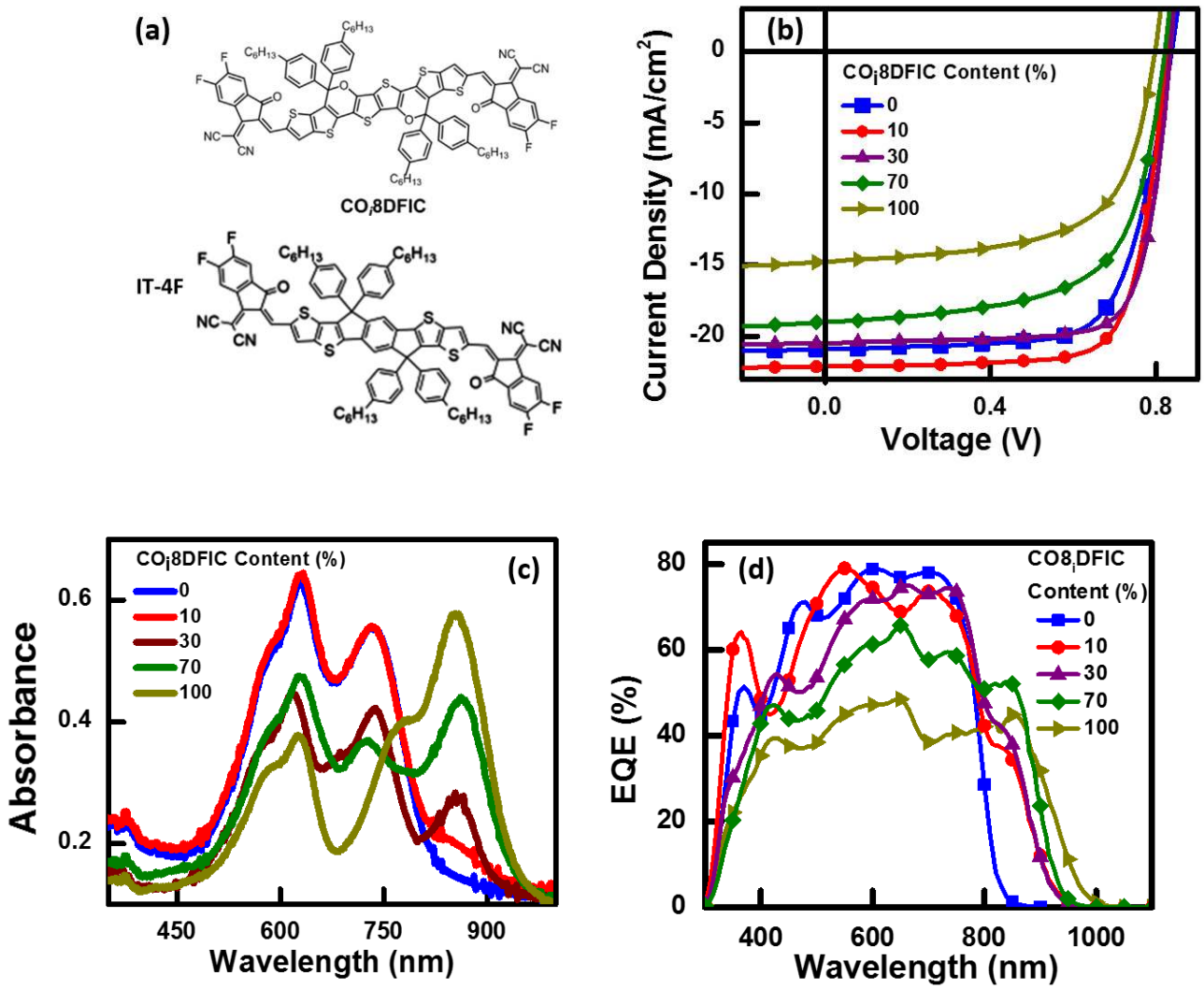

Figure 1. (a) Chemical structures of COi8DFIC and IT-4F; (b) JV curves; (c) thin film absorption spectra; and (d) EQE spectra of PBDB-T-2F-based solar cells with different COi8DFIC contents.

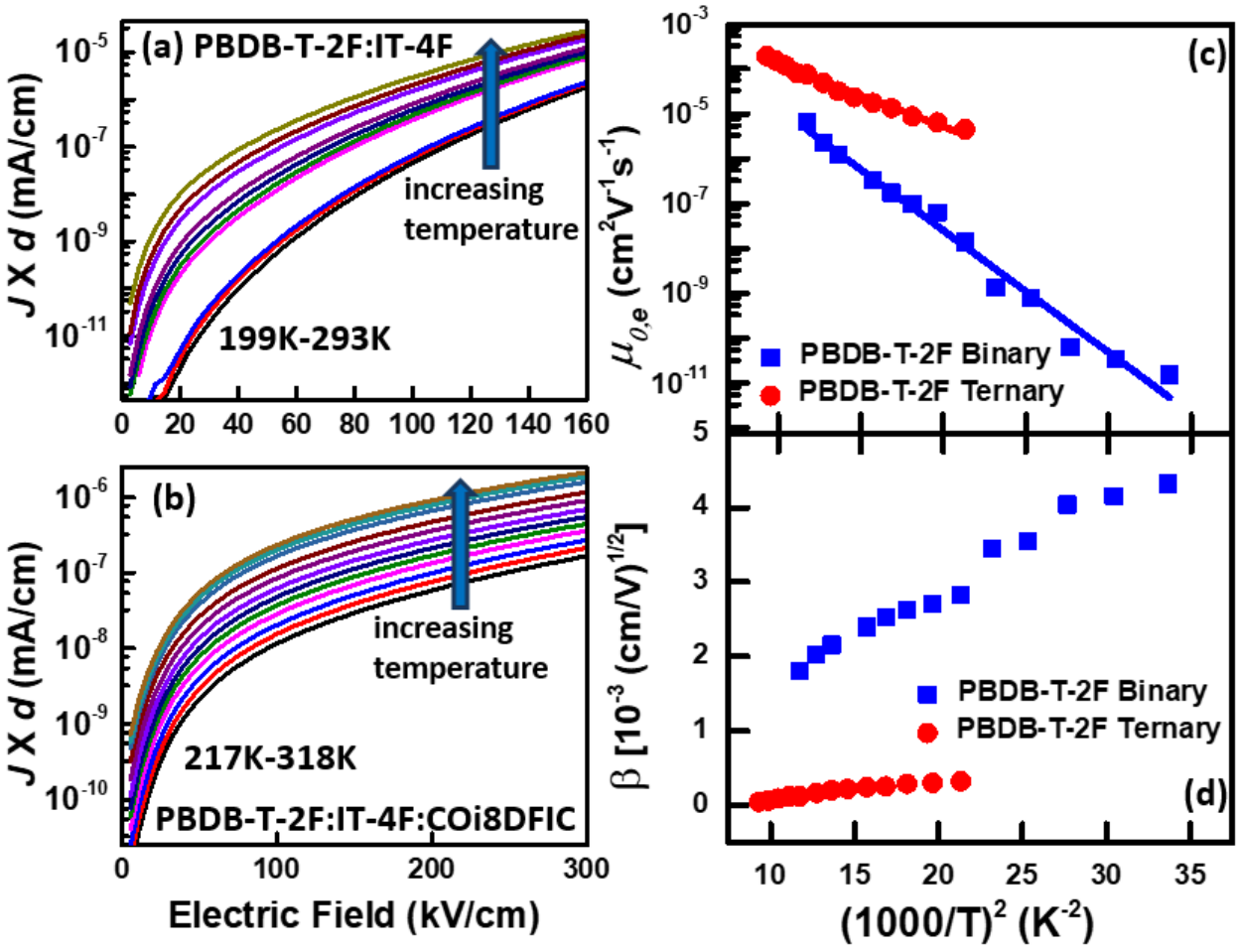

Figure 2. Electron-only currents of (a) PBDB-T-2F:IT-4F and (b) PBDB-T-2F:IT-4F:COi8DFIC (10 wt% COi8DFIC) BHJ devices at different temperatures; (c) zero-field electron mobilities and (d) Poole-Frenkel slopes extracted from (a) and (b), as a function of the device temperature.

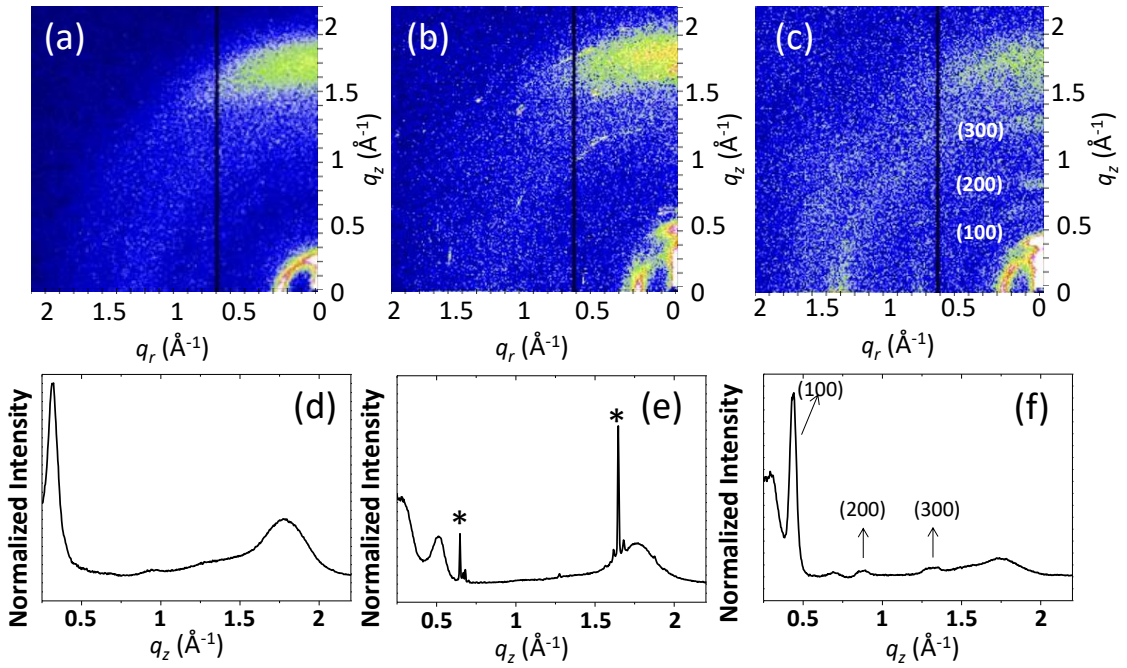

Figure 3. GIWAXS patterns for (a) binary PBDB-T-2F:IT-4F, (b) binary PBDB-T-2F:COi8DFIC and (c) ternary PBDB-T-2F:IT-4F:COi8DFIC BHJ thin films. GIWAXS out-of-plane profiles of (d) binary PBDB-T-2F:IT-4F, (e) binary PBDB-T-2F:COi8DFIC, and (f) ternary PBDB-T-2F:IT-4F:COi8DFIC BHJ thin films.

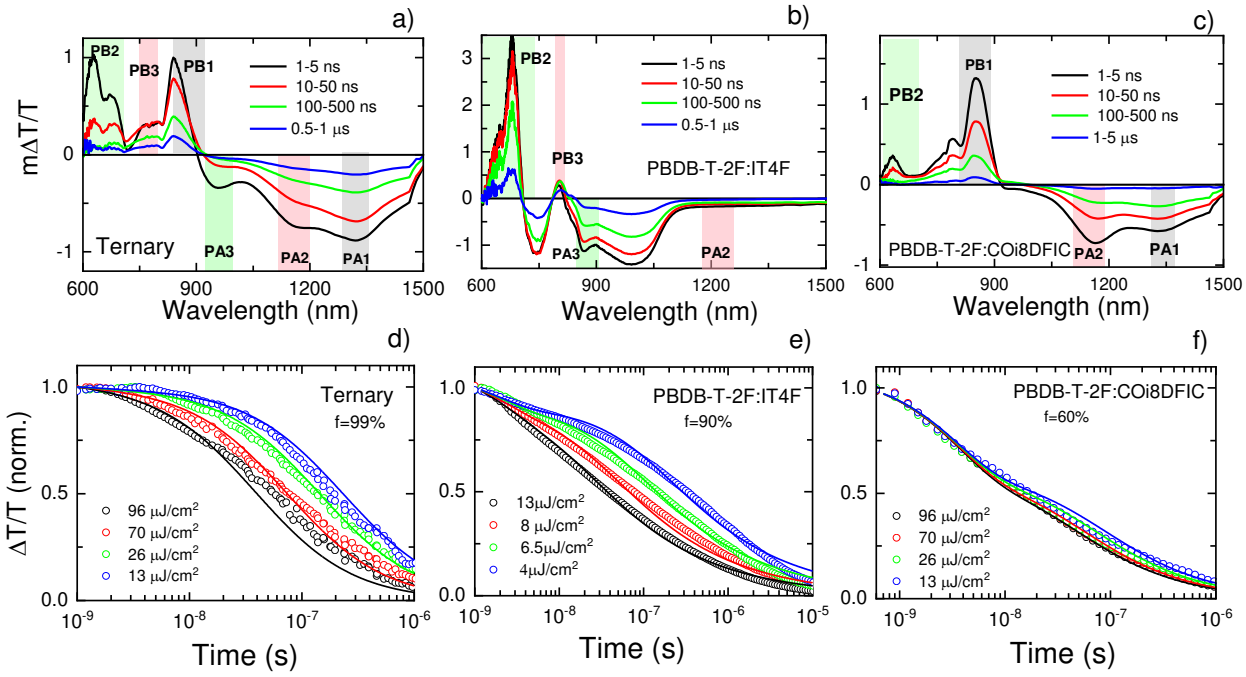

Figure 4. ns-μs TA spectra of a) ternary, (b) PBDBT-2F:IT4F, and (c) PBDBT-2F:COi8DFIC BHJ thin films. ns-μs TA decay dynamics of charge carriers for at different fluences (d-f). Two-pool fits (solid lines) of the experimentally-measured carrier dynamics (open symbols) of ternary (d), PBDB-T-2F:IT4F (e), and PBDB-T-2F:COi8DFIC (f) blends, respectively. From the fit, the charge separation efficiency was determined to 99% (ternary BHJ), 90% (PBDB-T-2F:IT4F), and 60% (PBDB-T-2F:COi8DFIC).

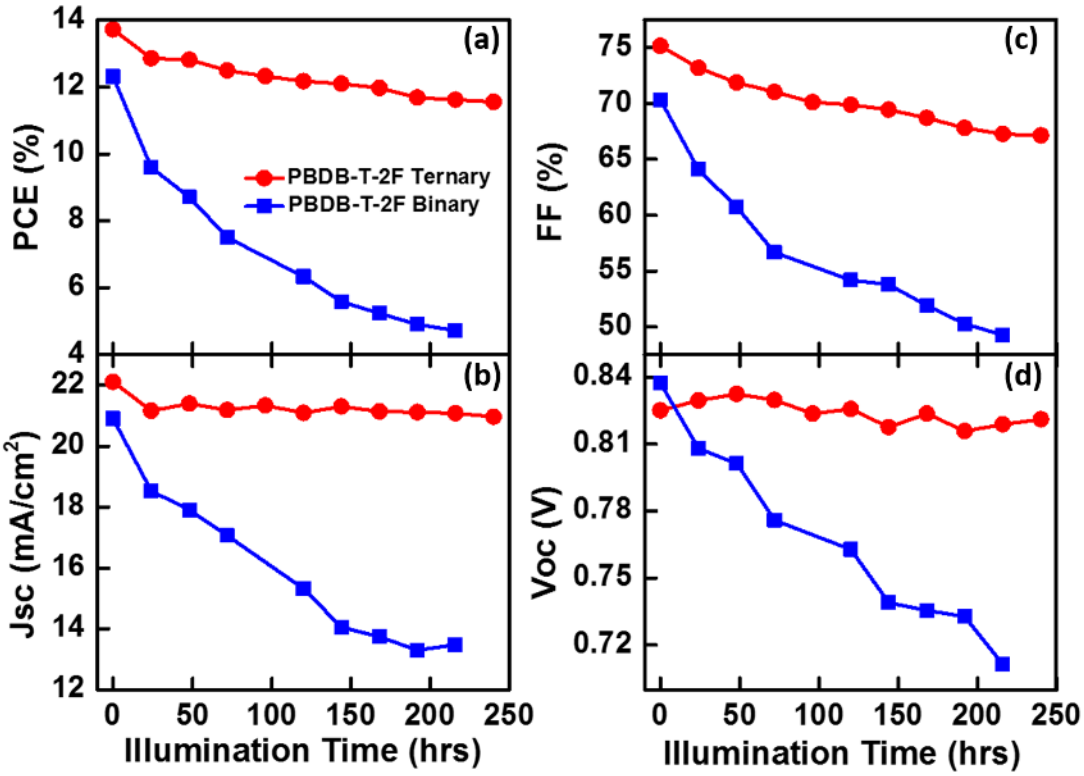

Figure 5. OPV device parameters: (a) PCE, (b) J_{sc}, (c) FF, and (d) V_{oc} of binary PBDB-T-2F:IT-4F and ternary PBDB-T-2F:IT-4F:COi8DFIC (10 wt% COi8DFIC) BHJ solar cells as a function of the exposure time to 1-sun illumination.

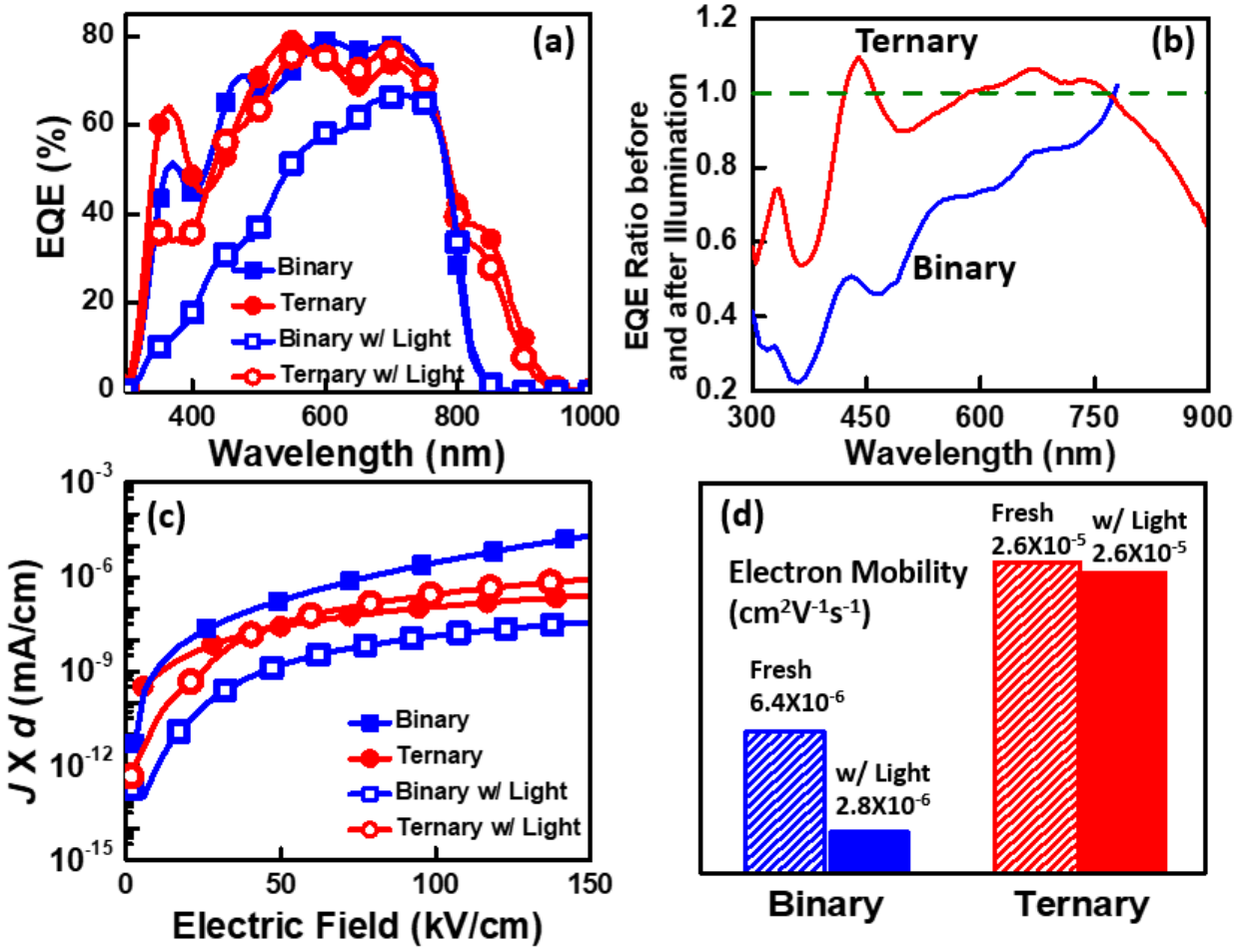

Figure 6. (a) EQE spectra; (b) EQE ratios before and after a 120-hour illumination. The dashed line in (b) is a guide to distinguish between increased (>1) and decreased (<1) EQE values after illumination. (c) electron-only JV curves of the binary PBDB-T-2F:IT-4F and ternary PBDB-T-2F:IT-4F:COi8DFIC (10 wt% COi8DFIC) BHJs immediately after preparation and after 120-hour of 1-sun illumination. Corresponding charge carrier mobilities are shown in (d).

AUTHOR INFORMATION

Corresponding Author

* Prof. Gang Li Email: gang.w.li@polyu.edu.hk

* Prof. Shu Kong So Email: skso@hkbu.edu.hk

* Prof. Frédéric Laquai Email: frederic.laquai@kaust.edu.sa

Author Contributions

G. L. conceptualized the project. G. L., S. K. S. and F. L. planed and supervised the project. Device fabrication/characterization, photostability test, and charge transport studies were carried out by H.Y. and C. Z. H. Y. participated in the detailed experimental design. Morphology analysis was performed by H.H.. Z.X. and L. D. synthesized COi8DFIC. S.K. performed the transient absorption spectroscopy experiments and data analysis. F.L. supervised the transient spectroscopy work. Device and film characterization were performed by H.T., L.C., P.F., Z.Z., Y.G. J.Y., C.Y. G.L., S.K.S., Y.G., J.Y., F.L. were responsible for the overall project direction. All authors have participated in the project and given approval and contributed to editing the final version of the manuscript. The manuscript was written through contributions of all authors. ‡These authors contributed equally.

Funding Sources

Research Grants Council of Hong Kong (Project Nos 15218517, C5037-18G), Shenzhen Science and Technology Innovation Commission (Project No. JCYJ20170413154602102); The funding for Project of Strategic Importance provided by the Hong Kong Polytechnic University (Project Code: 1-ZE29). Research Grant Council of Hong Kong under Grant # NSFC/RGC N-HKBU 202/16, and

the Research Committee of HKBU under Grant #RC-ICRS/15-16/4A-SSK. King Abdullah University of Science and Technology (KAUST).

ACKNOWLEDGMENT

G. Li thanks the support from Research Grants Council of Hong Kong (Project Nos 15218517, C5037-18G), Shenzhen Science and Technology Innovation Commission (Project No. JCYJ20170413154602102), and the funding for Project of Strategic Importance provided by the Hong Kong Polytechnic University (Project Code: 1-ZE29). SKS would like to acknowledge support from the Research Grant Council of Hong Kong under Grant # NSFC/RGC N-HKBU 202/16, and the Research Committee of HKBU under Grant #RC-ICRS/15-16/4A-SSK.The research reported in this publication was supported by funding from King Abdullah University of Science and Technology (KAUST).

REFERENCES

[1] . Günes, S.; Neugebauer, H.; Sariciftci, N. S., Conjugated Polymer-Based Organic Solar Cells. *Chem. Rev*. **2007**, *107*, 1324-1338.

[2] Li, G.; Zhu, R.; Yang, Y., Polymer Solar Cells. *Nat. Photonics.* **2012**, *6*, 153-161.

[3] Park, S. H.; Roy, A.; Beaupré, S.; Cho, S; Coates, N.; Moon, J. S.; Moses, D.; Leclerc, M.; Lee, K.; Heeger, A. J., Bulk Heterojunction Solar Cells with Internal Quantum Efficiency Approaching 100%. *Nat. Photonics* **2009**, *3*, 297-302.

[4] Tang, C. T., Two – Layer Organic Photovoltaic Cells. *Appl. Phys. Lett*. **1986**, *48*, 183.

[5] Li, G.; Chang, W.; Yang, Y., Low-Bandgap Conjugated Polymers Enabling Solution-Processable Tandem Solar Cells *Nat. Rev. Mater*. **2017**, *2*, 17043.

[6] Rowell, M. W.; Topinka, M. A.; McGehee, M. D., Organic Solar Cells with Carbon Nanotube Network Electrodes. *Appl. Phys. Lett*. **2006**, *88*, 233506.

[7] An, Q.; Zhang, F.; Zhang, J.; Tang, W.; Deng, Z.; Hu, B., Versatile Ternary Organic Solar Cells: A Critical Review. *Energy Environ. Sci*. **2016**, *9*, 281-322.

[8] Yan, C.; Barlow, S.; Wang, Z.; Yan, H.; Jen, A. K. Y.; Marder, S. R.; Zhan, X., Non – Fullerene Acceptors for Organic Solar Cells. *Nat. Rev. Mater*. **2018**, *3*, 18003.

[9] Erb, T.; Zhokhavets, U.; Gobsch, G.; Raleva, S.; Stühn, B.; Schilinsky, P.; Waldauf, C.; Brabec, C. J., *Adv. Function. Mater*. **2005**, *15*, 1193-1196.

[10] Yan, C.; Wang, W.; Lau, T.; Li, K.; Wang, J.; Liu, K.; Lu, X.; Zhan, X., Enhancing the Performance of Non-Fullerene Organic Solar Cells via End Group Engineering of Fused-Ring Electron Acceptors, *J. Mater. Chem. A* **2018**, *6*, 16638-16644; Yan, C.; Yang, T.; Gao, W.; Xiao, Y.; Li, Y.; Lu, X.; Yang, C.; Li, G., Chlorination Strategy Induced Abnormal Nanomorphology Tuning in High Efficiency Organic Solar Cells – A Study of Phenyl Substituted Benzodithiophene Based Non-Fullerene Acceptors. *Sol. RRL* **2019** 10.1002/solr.201900262.

[11] Li, G.; Shrotriya, V.; Huang, J.; Yao, Y.; Moriarty, T.; Emery, K.; Yang, Y., High-Efficiency Solution Processable Polymer Photovoltaic Cells by Self – Organization of Polymer Blends. *Nat. Mater*. **2005**, *4*, 864-868.

[12] Yang, Y.; Chen, W.; Dou, L.; Chang, W. H.; Duan, H. S.; Bob, B.; Li, G.; Yang, Y., High-Performance Multiple-Donor Bulk Heterojunction Solar Cells *Nat. Photonics* **2015**, *9*, 190-198;

Huang, W, Cheng, P, Yang, Y, Li, G, Yang, Y, High‐Performance Organic Bulk‐Heterojunction Solar Cells Based on Multiple‐Donor or Multiple‐Acceptor Components. *Adv. Mater*. **2018**, 30, 1705706.

[13] Cui, Y.; Yao, H.; Hong, L.; Zhang, T.; Xu, Y.; Xian, K.; Gao, B.; Qin, J.; Zhang, J.; Wei, Z.; Hou, J., Achieving Over 15% Efficiency in Organic Photovoltaic Cells via Copolymer Design, *Adv. Mater*. **2019**, *31*, 1808356.

[14] Yuan, J.; Zhang, Y.; Zhou, L.; Zhang, G.; Yip, H. L.; Lau, T.; Lu, X.; Zhu, C.; Peng, H.; Johnson, P. A.; Leclerc, M.; Cao, Y.; Ulanski, J.; Li, Y.; Zou, Y., Single-Junction Organic Solar Cell with over 15% Efficiency Using Fused-Ring Acceptor with Electron - Deficient Core. *Joule* **2019**, *3*, 1140-1151.

[15] Meng, L.; Zhang, Y.; Wan, X.; Li, C.; Zhang, X.; Wang, Y.; Ke, X.; Xiao, Z.; Ding, L.; Xia, R.; Yip, H. L.; Cao, Y.; Chen, Y., Organic and Solution – Processed Tandem Solar Cells with 17.3% Efficiency. *Science* **2018**, *361*, 1094-1098.

[16] Shaheen, S. E.; Brabec, C. J.; Sariciftci, N. S., 2.5% Efficient Organic Plastic Solar Cells. *Appl. Phys. Lett*. **2001**, *78*, 841.

[17] Yin, H.; Bi, P.; Cheung, S. H.; Cheng, W. L.; Chiu, K. L.; Ho, C. H. Y.; Li, H. W.; Tsang, S. W.; Hao, X.; So, S. K., Balanced Electric Field Dependent Mobilities: A Key to Access High Fill Factors in Organic Bulk Heterojunction Solar Cells. *Solar RRL* **2018**, *2*, 1700239.

[18] Fei, Z.; Eisner, F. D.; Jiao, X.; Azzouzi, M.; Röhr, J. A.; Han, Y.; Shahid, M.; Chesman, A. S. R.; Easton, C. D.; McNeill, C. R.; Anthopoulos, T. D.; Nelson, J.; Heeney, M., An Alkylated Indacenodithieno[3,2-b]thiophene-Based Nonfullerene Acceptor with High Crystallinity

Exhibiting Single Junction Solar Cell Efficiencies Greater than 13% with Low Voltage Losses. *Adv. Mater*. **2018**, *30*, 1705209.

[19] Duan, T.; Tang, H.; Liang, R.; Lv, J.; Kan, Z.; Singh, R.; Kumar, M.; Xiao, Z.; Lu, S.; Laquai, F., Terminal Group Engineering for Small-Molecule Donors Boosts the Performance of Nonfullerene Organic Solar Cells. *J. Mater. Chem. A* **2019**, *7*, 2541-2546.

[20] Dayneko, S.V.; Hendsbee, A. D.; Welch, G. C., Combining Facile Synthetic Methods with Greener Processing for Efficient Polymer-Perylene Diimide Based Organic Solar Cells. *Small Methods* **2018**, *2*, 1800081.

[21] An, Q.; Zhang, F.; Gao, W.; Sun, Q.; Zhang, M.; Yang, C.; Zhang, J., High-efficiency and air stable fullerene-free ternary organic solar cells. *Nano Energy* **2018**, *45*, 177-183.

[22] Kawano, K.; Pacios, R.; Poplavskyy, D.; Nelson, J.; Bradley, D. D. C.; Durrant, J. R., Degradation of Organic Solar Cells due to Air Exposure. *Sol. Energy Mater. Sol. C*. **2006**, *90*, 3520-3530.

[23] Cheng, P.; Zhan, X., Stability of Organic Solar Cells: Challenges and Strategies. *Chem. Soc. Rev*. **2016**, *45*, 2544-2582.

[24] Hoppe, H.; Sariciftci, N. S., Organic Solar Cells: A Review. *J. Mater. Res*. **2004**, *19*, 1924-1945.

[25] Zhu, W.; Wu, Y.; Wang, S.; Li, W.; Li, X.; Chen, J.; Wang, Z.; Tian, H., Organic D-A-π-A Solar Cell Sensitizers with Improved Stability and Spectral Response. *Adv. Function. Mater*. **2011**, *21*, 756-763.

[26] Xiao, Z.; Jia, X.; Ding, L., Ternary Organic Solar Cells Offer 14% Power Conversion Efficiency. *Sci. Bul*. **2017**, *62*, 1562-1564.

[27] Dai, S.; Li, T.; Wang, W.; Xiao, Y.; Lau, T.; Li, Z.; Liu, K.; Lu, X.; Zhan, X., Enhancing the Performance of Polymer Solar Cells via Core Engineering of NIR-Absorbing Electron Acceptors. *Adv. Mater*. **2018**, *30*, 1706571.

[28] Xiao, Z.; Jia, X.; Li, D.; Wang, S.; Geng, X.; Liu, F.; Chen, J.; Yang, S.; Russell, T. P.; Ding, L., 26 $mAcm^{-2}$ J_{sc} from Organic Solar Cells with a Low-Bandgap Nonfullerene Acceptor. *Sci. Bul*. **2017**, *62*, 1494-1496.

[29] Ho, C. H. Y.; Cao, Lu, Y.; Lau, T.; Cheung, S. H.; Li, H.; Yin, H.; Chiu, K. L.; Ma, L.; Cheng, Y.; Tsang, S.; Lu, X.; So, S. K.; Ong, B. S., Boosting the Photovoltaic Thermal Stability of Fullerene Bulk Heterojunction Solar Cells through Charge Transfer Interactions *J. Mater. Chem. A* **2017**, *5*, 23662-23670.

[30] Yin, H.; Chen, S.; Bi, P.; Xu, X.; Cheung, S. H.; Hao, X.; Peng, Q.; Zhu, X.; So, S. K., Rationalizing Device Performance of Perylenediimide Derivatives as Acceptors for Bulk-Heterojunction Organic Solar Cells. *Org. Electron*. **2019**, *65*, 156-161.

[31] Yin, H.; Chen, S.; Cheung, S. H.; Li, H. W.; Xie, Y.; Tsang, S. W.; Zhu, X.; So, S. K., Porphyrin-Based Thick-Film Bulk-Heterojunction Solar Cells for Indoor Light Harvesting. *J. Mater. Chem. C* **2018**, *6*, 9111-9118.

[32] Ho, C. Y. H.; Cheung, S. H.; Li, H. W.; Chiu, K. L.; Cheng, Y.; Yin, H.; Chan, M. H.; So, F.; Tsang, S. W.; So, S. K., Using Ultralow Dosages of Electron Acceptor to Reveal the Early Stage Donor–Acceptor Electronic Interactions in Bulk Heterojunction Blends. *Adv. Energy Mater*. **2017**, *7*, 1602360.

[33] Yin, H.; Cheung, S. H.; Ngai, J. H. L.; Ho, C. H. Y.; Chiu, K. L.; Hao, X.; Li, H. W.; Cheng, Y.; Tsang, S. W.; So, S. K., Thick-Film High-Performance Bulk-Heterojunction Solar Cells Retaining 90% PCEs of the Optimized Thin Film Cells. *Adv. Electron. Mater*. **2017**, *3*, 1700007.

[34] Karuthedath, S.; Melianas, A.; Kan Z.; Pranculis, V.; Wohlfahrt, M.; Khan, J. I.; Gorenflot, J.; Xia, Y.; Inganäs, O.; Gulbinas, V.; Kemerink, M.; Laquai, F.; Thermal Annealing Reduces Geminate Recombination in TQ1:N2200 All-Polymer Solar Cells. *J. Mater. Chem. A* **2018**, *6*, 7428-7438.

[35] Howard, I. A.; Mauer, R.; Meister, M.; Laquai, F.; Effect of Morphology on Ultrafast Free Carrier Generation in Polythiophene:Fullerene Organic Solar Cells. *J. Am. Chem. Soc*. **2010**, *132*, 14866-14876.

[36] Karuthedath, S.; Gorenflot, J.; Firadus, Y.; Sit, W. Y.; Eisner, F.; Seitkhan, A.; Ravva, M. K.; Anthopoulos, T. D.; Laquai, F.; Charge and Triplet Exciton Generation in Neat $PC_{70}BM$ Films and Hybrid CuSCN:PC70BM Solar Cells. *Adv. Energy Mater*. **2019**, *9*, 1802476.

BRIEFS (Word Style “BH_Briefs”). If you are submitting your paper to a journal that requires a brief, provide a one-sentence synopsis for inclusion in the Table of Contents.

SYNOPSIS (Word Style “SN_Synopsis_TOC”). If you are submitting your paper to a journal that requires a synopsis, see the journal’s Instructions for Authors for details.

For Table of Contents Only